Electrical conductivity, thermopower and ^{57}Fe Mössbauer spectroscopy of solid solutions $Fe(Nb_{1-x}W_x)O_4$, $0 \leqslant x \leqslant 0.4$

1998 J. Phys.: Condens. Matter 10 8279

(http://iopscience.iop.org/0953-8984/10/37/014)

J. Phys.: Condens. Matter **10** (1998) 8279–8292. Printed in the UK PII: S0953-8984(98)90453-2

Electrical conductivity, thermopower and ^{57}Fe Mössbauer spectroscopy of solid solutions $Fe(Nb_{1-x}W_x)O_4$, $0 \leqslant x \leqslant 0.4$

E Schmidbauer

Institut für Allgemeine und Angewandte Geophysik der Universität München, Theresienstrasse 41, 80333 München, Germany

Received 7 January 1998, in final form 13 June 1998

Abstract. Electrical conductivity and thermopower data are presented for sintered semiconducting compositions $Fe(Nb_{1-x}W_x)O_4$, $0 \leqslant x \leqslant 0.4$, where charge transport is thought to be effected by electron hopping $Fe^{2+} \rightarrow Fe^{3+}$. The extrapolated crystallite DC conductivity σ was measured between ~100 and 300 K using impedance spectroscopy (20 Hz–1 MHz), with typical values of $\sigma(300\ \mathrm{K}) = 10^{-2}$–$10^{-1}\ \Omega^{-1}\ \mathrm{cm}^{-1}$. The results can be approximated reasonably well by the relation $\sigma \propto \exp[-(T_0/T)^{1/4}]$ at not too low temperatures. The thermopower Θ is negative (n-type conduction) in the range ~100–900 K and shows below ~300 K a temperature variation of approximately $\Theta \propto T^{1/2}$, while it becomes largely temperature independent above ~300 K. From the latter data the concentration ratio $[Fe^{2+}]/[Fe^{3+}]$ for Fe ions taking part in charge transport can be derived; this is compared with that determined from ^{57}Fe Mössbauer spectra at low temperatures which encompasses all Fe cations. There appears to be a certain correlation with the change at $x \sim 0.1$, which is possibly related to electron correlation effects for larger x-values.

1. Introduction

Solid solutions $Fe(Nb_{1-x}W_x)O_4$, $0 \leqslant x \leqslant 1$, with the wolframite crystal structure (space group $P2/c$) exhibit mixed valencies Fe^{2+} and Fe^{3+} in the composition range $0 < x < 1$ [1]. Such a situation can give rise to a conduction process by electron transfer $Fe^{2+} \rightarrow Fe^{3+}$ between neighbouring Fe cations that has been found in several mixed crystal series, preferentially of spinel ferrites, where in part a thermally activated electron hopping mechanism has been established to govern conductivity; frequently, charge localization is generated or enhanced by cation disorder that gives rise to random fields [2–10].

The monoclinic (pseudo-rhombic) wolframite structure is characterized by two kinds of zig-zag chains of edge-sharing MeO_6 octahedra (Me = Fe, Nb, W) along the [001] direction. One chain consists of FeO_6 octahedra and the second one of $(Nb, W)O_6$; both kinds of chains alternate along [100]. Typical features of the wolframite lattice are illustrated in figure 1. The series offers the opportunity to have available zig-zag chains of $(Fe^{2+}, Fe^{3+})O_6$ octahedra along [001] throughout the whole series provided ordering of both kinds of chains is complete. Thus, a possibly dominating one-dimensional conduction along the chains may occur with $Fe^{2+} \rightarrow Fe^{3+}$ electron exchange across octahedral edges (figure 1), or via O^{2-} anions; in the latter case, interchain conductivity can be thought of by this kind of charge transfer. The above charge transport can be affected by vacancies, impurities and other

0953-8984/98/378279+14$19.50

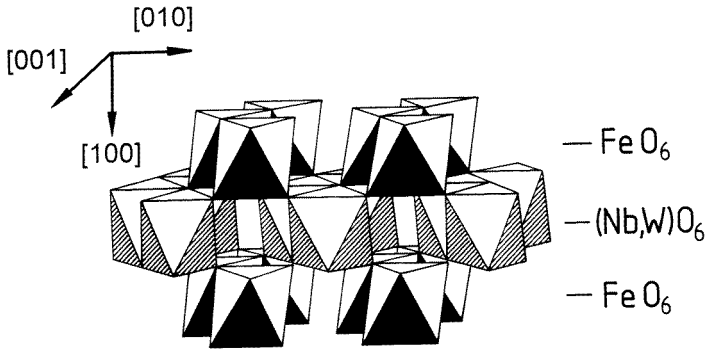

Figure 1. Typical features of the wolframite structure; FeO_6 and $(Nb, W)O_6$ octahedra are ordered in chains along the [001] direction.

defects that may act as donors or acceptors; in addition, a further independent conduction process can be superposed.

The electrical conductivity σ of all compositions was found to show a semiconducting behaviour with non-linear $\log\sigma$–$1/T$ curves and activation energies $E_A(350\ \mathrm{K}) \sim 0.17$–$0.55$ eV [1]; the conduction mechanism was thought to be governed by an electron hopping process between Fe^{2+} and Fe^{3+}. For stoichiometric compositions of the above series, a gradual change in the concentrations of Fe^{3+} and Fe^{2+} occurs in the range $0 < x < 1$ where the theoretical compositions of the end members is $Fe^{3+}Nb^{5+}O_4$ ($x = 0$) and $Fe^{2+}W^{6+}O_4$ ($x = 1$), and the formula $Fe^{3+}_{1-x}Fe^{2+}_x(Nb^{5+}_{1-x}W^{6+}_x)O^{2-}_4$ is valid. A maximum σ at $x = 0.6$ was found, where $\sigma(294\ \mathrm{K}) \sim 5 \times 10^{-2}\ (\Omega\ \mathrm{cm})^{-1}$ [1]. For not too large x, the content of Fe^{3+} is dominating and that of Fe^{2+} is low; the conduction is of n-type [1] and σ is given by $\sigma = en\langle\mu_D\rangle$, where e is the electronic charge, n the concentration of charge carriers and $\langle\mu_D\rangle$ the average drift mobility. In compositions of the series the electron transfer $Fe^{2+} \rightarrow Fe^{3+}$ was found to be sensed by Mössbauer spectra [11] and by XANES results [12].

We have examined the behaviour of electrical transport properties of sintered compositions $0 \leqslant x \leqslant 0.4$ between ~100 and 900 K, using DC/AC conductivity and thermopower data, in order to elucidate the conduction processes in more detail. Impedance spectroscopy was applied as it was thought to enable the distinction between crystal and grain boundary conductivities. In order to check stoichiometry, ^{57}Fe Mössbauer spectroscopy was used to determine the concentration ratios $[Fe^{2+}]/[\Sigma Fe]$, as a possible oxygen non-stoichiometry changes the ratio.

2. Samples and experimental methods

Polycrystalline samples with compositions $x = 0$, 0.05, 0.1, 0.2, 0.3 and 0.4 were prepared by the solid-state reaction of mixtures of α-Fe_2O_3 (99.995%), Nb_2O_5 (99.998%) and WO_3 (99.995%) powders. Adequate mixtures were milled, compacted and subjected to presintering at ~950–1000 °C for ~20 h at varying oxygen partial pressures p_{O_2}, depending on composition. After crushing, regrinding and repressing (~2 kbar), a final sintering process was carried out for all compositions at ~1200 or 1300 °C for ~50 h at varying p_{O_2} values. No exact equilibrium p_{O_2} values are known and hence estimated values were used for the final sintering procedure. Samples applied for measurements were slowly cooled

to room temperature by switching off the furnace; they were found to be single phase. Compositions and preparation conditions are listed in table 1.

Table 1. Heating conditions for the final heating procedure of compositions $Fe(Nb_{1-x}W_x)O_4$; p_{O_2} = oxygen partial pressure. Furnace cooling was to room temperature in ∼8 h without changing the gas atmosphere or the gas mixture.

x	T (°C)	p_{O_2} (at)
0	1300	$10^{-0.68}$ (air)
0.05	1200	$10^{-0.68}$
0.1	1200	$10^{-0.68}$
0.2	1200	$10^{-1.48}$ (N_2/O_2)
0.3	1200	$10^{-2.60}$
0.4	1200	$10^{-3.84}$ (CO_2)

X-ray analysis was performed for all samples used for electrical measurements. For this purpose, the Rietveld refinement technique was utilized, indexing all compositions on a wolframite structure as known for $FeWO_4$ [13, 14]. Lattice parameters are listed in table 2. They are in satisfactory agreement with the results presented by [1, 11]. Cation separations Fe–Fe (and Me–Me (Me = Nb, W)) are typically ∼0.32 nm, which is far above the distance allowing itinerant electron transfer in transition metal oxides. Light microscopic analyses of all samples showed a variation of porosity p with composition, which became increasingly larger with rising x, with $p = 0.05$–0.15. The average crystallite size was 20–50 μm.

Table 2. Lattice parameters of the wolframite lattice (space group $P2/c$) deduced from x-ray diffractograms for compositions $Fe(Nb_{1-x}W_x)O_4$.

x	a (nm)	b (nm)	c (nm)	β (°)
0	0.4650(3)	0.5631(5)	0.5007(6)	90.27
0.05	0.4652(7)	0.5632(5)	0.5004(8)	90.12
0.1	0.4655(4)	0.5638(7)	0.4999(3)	90.07
0.2	0.4659(3)	0.5647(6)	0.5006(9)	90.03
0.3	0.4663(5)	0.5653(8)	0.5001(6)	90.01
0.4	0.4667(7)	0.5659(5)	0.4997(4)	90.01

2.1. ^{57}Fe Mössbauer spectra

Spectra for compositions $x = 0$, 0.05, 0.1, 0.2, 0.3, 0.4 with the wolframite structure were recorded between 294 and 80 K. Typical spectra are seen from figure 2 for $x = 0.1$, 0.3, 0.4 that are in agreement with patterns recorded earlier [1, 11]. Spectra at ∼80 K could be fitted adequately using three doublets, as also applied in [11]. For each pattern, the strong doublet with the small quadrupole splitting (QS) and low isomer shift (IS) (with reference to metallic Fe) is typical for Fe^{3+}. The other doublets arise doubtless from two groups of Fe^{2+} that are characterized by a large IS ∼ 1.2 mm s^{-1}, with the exception of $x = 0$ where no other doublets could be observed within the error of measurement [15]; the doublet with the larger QS reveals a rather small linewidth B, indicating a group of Fe^{2+} with quite similar near-neighbour environments. In contrast, the larger B of the second kind of Fe^{2+} is typical for a strong variation of local environments. It is probable that both kinds of Fe^{2+} in an FeO_6 chain are associated with the arrangement of W^{6+} and Nb^{5+} in neighbouring

$(W^{6+}, Nb^{5+})O_6$ chains and/or with a deviation from full oxygen stoichiometry. The same assignments could be made for 137 K spectra. At higher T, as for instance at ∼295 K, in figure 2 similar spectra are recorded for $x = 0.3$ and 0.4, but Fe^{2+} doublets with narrow lines could no longer be recognized. Most probably, for each spectrum a distribution of $QS(Fe^{2+})$ exists with a variation of T dependences which we approximate by one doublet; it turned out that a fit as for ∼80 K patterns led to an enhanced error and by far the best free fit was attained with subspectra as visible from figure 2. Apart from typical Fe^{3+} and Fe^{2+} doublets, for each pattern there is a further doublet with IS ∼ 0.75 mm s^{-1}, which is a value that is intermediate between that for Fe^{3+} and Fe^{2+}, as also observed in [1, 11]; such a doublet has also been observed in spinel ferrites with mixed Fe^{2+}/Fe^{3+} and it was attributed to local electron hopping between Fe^{2+} and Fe^{3+} with hopping times $\tau < 10^{-8}$ s [16]. Mössbauer parameters are quoted in table 3; here, the last mentioned subspectra were also designated for the sake of brevity as Fe^{2+} doublets instead of $Fe^{2+/3+}$.

Table 3. Mössbauer parameters for subspectra of compositions $Fe(Nb_{1-x}W_x)O_4$, $x = 0.1$, 0.3, 0.4 at two temperatures. QS = quadrupole splitting, IS = isomer shift (relative to metallic Fe), B = linewidth; all data are given in mm s^{-1} with an accuracy of ±0.02 mm s^{-1}; $[Fe^{2+}]/[\Sigma Fe]$ from area ratios of subspectra are given to ∼±5%.

		QS			IS			B			$[Fe^{2+}]/[\Sigma Fe]$	
x	T (K)	Fe_1^{2+}	Fe_2^{2+}	Fe^{3+}	Fe_1^{2+}	Fe_2^{2+}	Fe^{3+}	Fe_1^{2+}	Fe_2^{2+}	Fe^{3+}	Expr.	Theor.
0.1	82	2.75	2.18	0.46	1.24	1.20	0.53	0.29	0.59	0.34	0.11	0.10
0.3	80	2.67	1.92	0.55	1.26	1.27	0.53	0.34	0.62	0.36	0.33	0.30
0.3	295	1.53	0.86	0.50	1.07	0.70	0.47	0.64	0.48	0.36	—	—
0.4	82	2.58	1.90	0.55	1.23	1.24	0.53	0.33	0.60	0.35	0.43	0.40
0.4	295	1.55	0.92	0.53	1.09	0.76	0.48	0.58	0.46	0.38	—	—

To determine concentration ratios $[Fe^{2+}]/[\Sigma Fe]$ from area ratios of ∼80 K subspectra, all f-factors were assumed to be identical. It appears that within the error of measurement the observed ratios are rather close to those expected for compositions with full oxygen stoichiometry (table 3). However, a reduced oxygen deficiency cannot be excluded for any composition, as is found also for many transition metal oxides; in this case there is a surplus in Fe^{2+} for charge compensation. The magnitude of $QS(Fe^{2+}) < 1.6$ mm s^{-1} at 294 K for $x = 0.3$ and 0.4 is rather low, which demonstrates a rapid decrease of QS with rising T, starting from the low-T region, where $QS(Fe^{2+}) \sim 2$–3 mm s^{-1}. This behaviour is in accord with $QS(T)$ data for $Fe^{2+}Nb_2O_6$ [17]; it signifies that the difference between the Fe^{2+} energy ground state and higher energy levels is comparatively small.

2.2. Experimental details

For AC conductivity measurements, a Hewlett Packard LCR-meter (HP4284A) was available, which operated in the frequency range 20 Hz–1 MHz. Impedance spectroscopy was applied plotting the real part Z' of the impedance against the imaginary part Z'' on the complex impedance plane [18]. For low-T measurements, a cryostat was used and at high T, a tube furnace; in the latter case, CO_2 was bubbled through a gas tight alumina tube for compositions $x > 0.2$, containing the sample holder and the samples.

Thermopower Θ data were recorded with a fully automatic device, using a computer controlled data acquisition system. At each selected T, adjusted by a T controller, five variable differences ΔT were generated between the sample faces, with a maximum

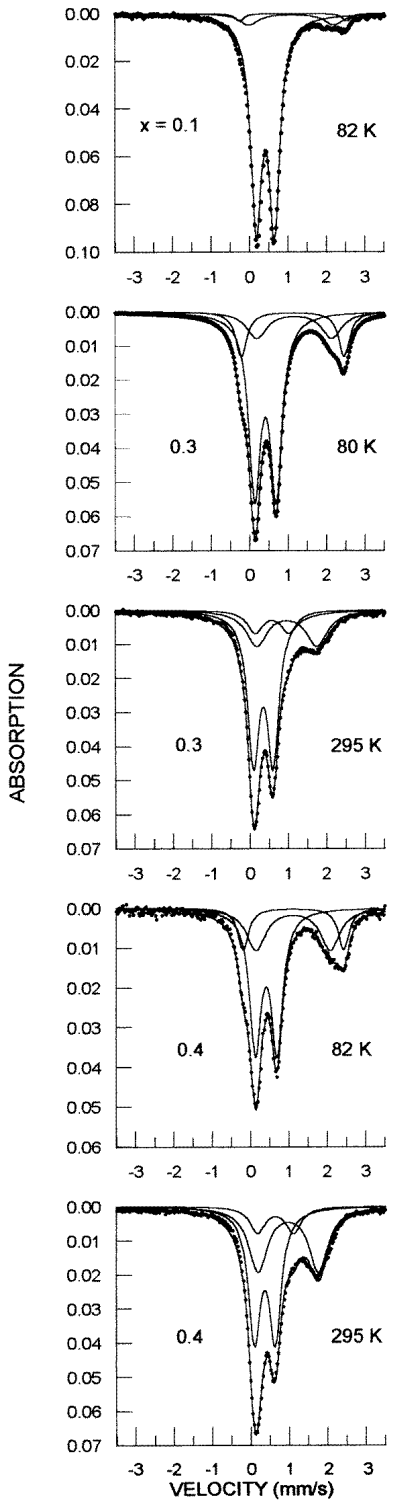

Figure 2. Mössbauer spectra for compositions $x = 0.1$ and 0.3 at various temperatures.

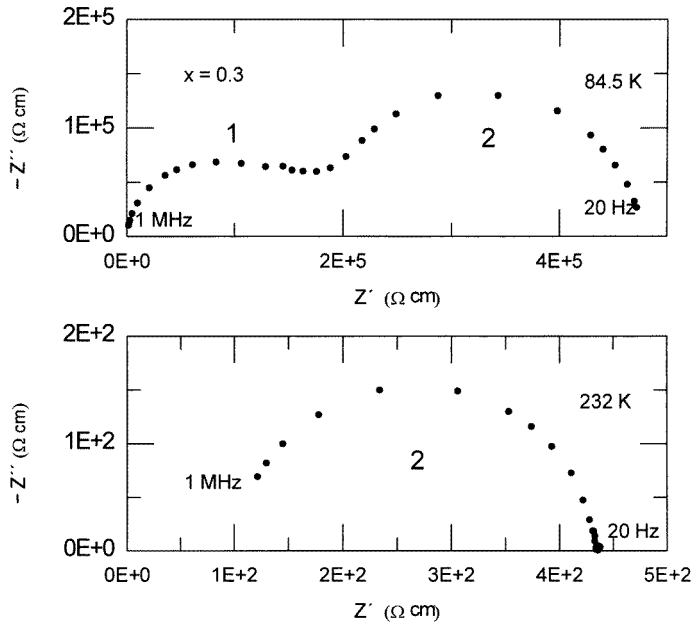

Figure 3. Typical impedance plots in the complex impedance plane.

$\Delta T \sim 10$ K, by means of a miniheater close to one electrode. Five sets of thermovoltage U_{th}–ΔT data were determined and the slope of the resulting straight line was obtained by a least-squares fit. At all T values, a good linearity was noticed. At low T, Cu cylinders and Cu leads were used as electrodes; at high T, Pt cylinders and Pt leads were used. Two thermocouples, inside the cylinder electrodes monitored the sample T at both faces, with the sample spring-loaded between the cylinders. Opposite sample faces were coated with Ag paste or left without coating for $T > 300$ K. Absolute Θ values are given by subtracting Θ_{Pt} or Θ_{Cu} [19, 20] from the measured Θ results.

The samples were parallelepipeds, cut from the sintered pellets by a wire saw. Typical sample dimensions were $5 \times 2.5 \times 2.5$ mm^3. Prior to the measurements, the samples were ground and polished, in order to remove eventual undesired surface layers.

3. Results

3.1. Electrical conductivity σ

Figure 3 shows typical impedance plots (real part Z' against imaginary part Z'') on the complex impedance plane for a sample with $x = 0.3$ at two T values. The visible semicircular arcs can be approximated by semicircles with the centres slightly below the Z' axis [18]; for an arc, extrapolation on the Z' axis towards zero frequency marks the extrapolated DC resistivity for the conduction process associated with this arc. The semicircle close to the origin is due to crystallite conduction as a consequence of the low capacitance C ($\sim$1 pF cm^{-1}); the second semicircle, related to a much higher capacitance, arises from grain boundary effects as has been found from results with samples cut to half their original lengths that led to a 50% reduction of both semicircles. Thus, electrode

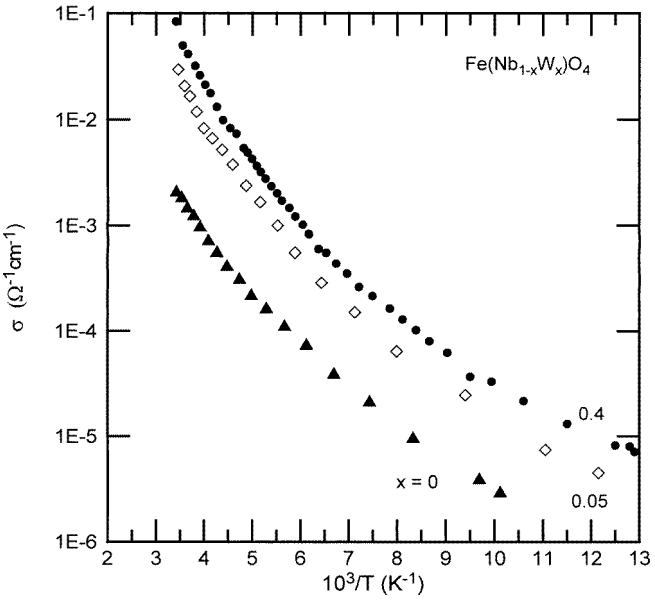

Figure 4. Logarithm of the extrapolated crystallite DC conductivity $\log\sigma$ against reciprocal temperature T^{-1} for various compositions.

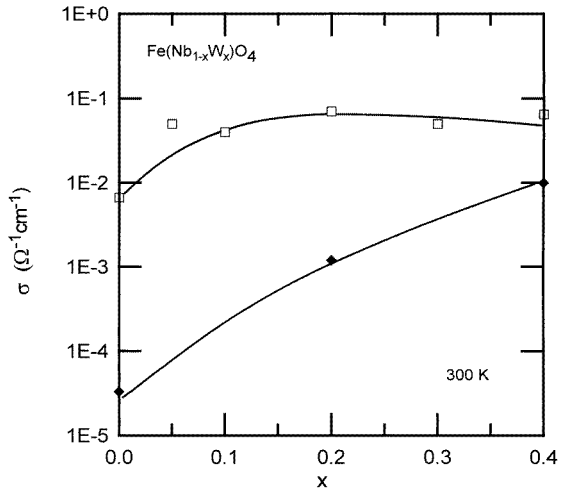

Figure 5. σ(300 K) as a function of composition x; □, our results; ⧫, data of [1].

effects were negligible. Both semicircular arcs were well developed for all samples. For $T \gtrsim 300$ K, only the sum of both mentioned resistivities could be measured. Thus, it was not possible to gain information of the crystallite conductivity and activation energy in the high-T limit well above 300 K.

Typical curves of the logarithm of the extrapolated DC conductivity $\log\sigma$ against $1/T$ for the crystallites are depicted in figure 4. Slightly bent curves are noted in the whole T range analysed. Data points for $x = 0.1$, 0.2 and 0.3 are between those for $x = 0.05$ and

0.4. Typical 'differential activation energies' close to room temperature are $E_A \sim 0.20$ eV and at the lowest T it is $E_A \sim 0.05$ eV. We found that very similar graphs are extrapolated for 'grain boundary' conduction related to the second circular arc of a Z'–Z'' diagram. Hence, it looks as if analogous charge transport processes are acting as in crystallites; also the deduced differential E_A values are similar. On the other hand, for $T > 300$ K, σ could only be determined for the sum of both resistivities, i.e. a superposition of at least two processes in a series circuit. In this case, for the high-T region up to ~800 K, a largely linear $\log\sigma$–$1/T$ relation was inferred, yielding $E_A = 0.25$–0.32 eV, well above the values for $T < 300$ K. Judging from the low-T behaviour of σ for the crystallites, these values may also serve as a certain measure for E_A of crystallites. Figure 5 shows, in addition, for the crystallites a plot of σ(300 K) against composition x along with data from [1]. There is a large difference between both data sets for $x \to 0$ which we ascribe in the first place to the fact that compositions of [1] were prepared in a gas stream of argon at the comparatively low temperature of 1000 °C which leads to a high sample porosity; a second point may be a variation of oxygen non-stoichiometry deviating probably from that for our samples.

We made an attempt to describe our data by a relation $\sigma \propto \exp[-(T_0/T)^x]$ with variable exponents ($\frac{1}{2}$, $\frac{1}{3}$ or $\frac{1}{4}$). It turned out that in limited T ranges the best fit was given with an exponent $x = 1/4$ (figure 6).

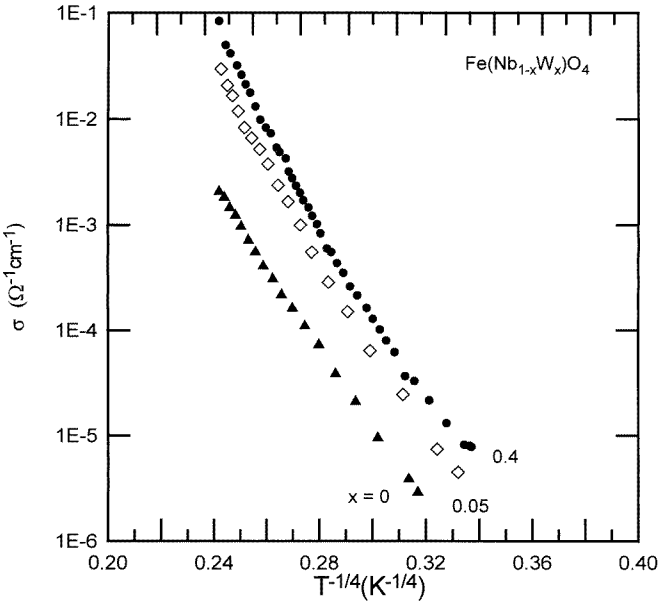

Figure 6. Logarithm of σ against $T^{-1/4}$ for the results of figure 5.

3.2. Thermopower Θ

Θ against temperature T plots are illustrated in figure 7 for $x = 0$, 0.05, 0.1, 0.2, 0.3 and 0.4 in a wide T range. Θ is negative for all samples, which implies n-type conduction. Below $T \sim 300$ K, a transition to a linear relation appears to take place for all compositions of the form $\Theta = AT + B$ or to a relationship $\Theta \propto T^{1/2}$, as required from some theoretical models in the low-T range; for a clear decision more accurate data points are necessary

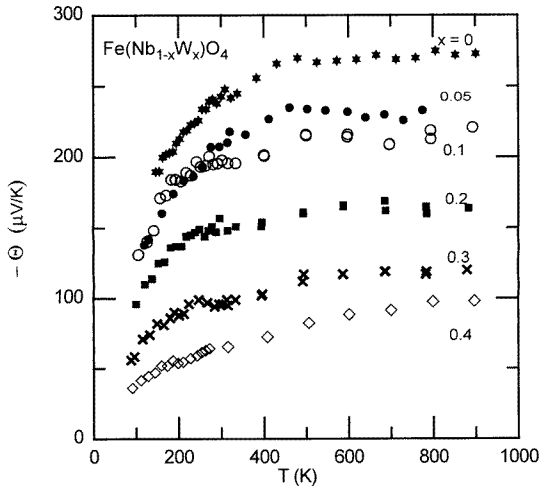

Figure 7. Thermopower Θ against T.

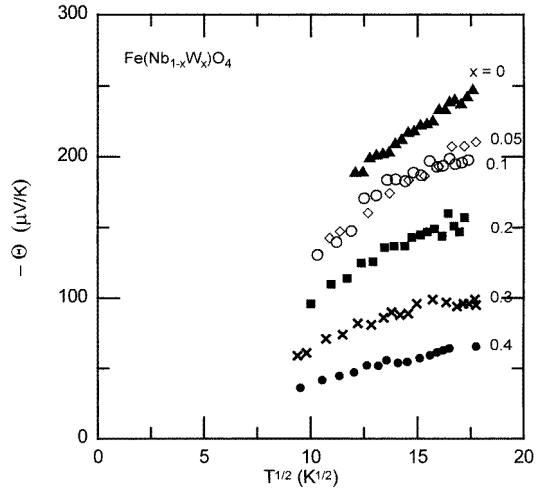

Figure 8. Thermopower Θ against $T^{1/2}$.

which range to lower T values. No such decrease in $|\Theta|$ has been noted for $FeWO_4$ ($x = 1$) [21]. In figure 8, we tentatively present our results in the form Θ–$T^{1/2}$ for $T \lesssim 300$ K; it appears in fact that an extrapolation $T \to 0$ may result in $\Theta \to 0$ for all samples, as required. At present, measurements cannot be extended to lower T because of too high sample resistivities. In principle, a single hopping mechanism can give rise to such a result with a broad transition region between both T ranges. The very similar results for $x = 0.05$ and 0.1 in figure 7, in particular at low T, is probably related to the fact that both compositions were sintered in air and, hence, at least one may deviate more from oxygen stoichiometry.

In the high-T range, a saturation of Θ takes place with increasing T. Such a behaviour is expected for hopping-type charge transport in certain conditions [22]. In this situation, the charge carriers are considered to be small polarons which are assumed to have a

low drift mobility $\langle\mu_D\rangle$. We estimate $\langle\mu_D\rangle$ for composition $x = 0.05$, for instance, at ~300 K, using the relation $\sigma = en\langle\mu_D\rangle$ in the case of suggested $Fe^{2+} \rightarrow Fe^{3+}$ electron hopping. If all Fe sites are available for conduction, this leads with the experimental σ to $\langle\mu_D\rangle \sim 10^{-4}$ cm s^{-1} V^{-1} which is typical for small-polaron hopping charge transport where values much less than 0.1 cm s^{-1} V^{-1} are assumed [23].

4. Discussion

4.1. Mössbauer spectra

In the literature, for $Fe(Nb_{1-x}W_x)O_4$ solid solutions with $x = 0.2$, 0.4, 0.6 it was concluded from spectra, applying a three-doublet fit to a pattern, that one doublet was due to Fe with an intermediate valence state $Fe^{2+/3+}$; from the large variation of the isomer shift with T for this latter doublet the average valence variations for Fe with T were inferred [11]. This observation is in agreement with our fits for $x = 0.3$ and 0.4 spectra at 295 K. The electron transfer between Fe^{2+} and Fe^{3+} is probably a localized one, i.e. it may not contribute to long-range electron transport sensed by the extrapolated DC conductivity σ. In our compositions, $Fe^{2+/3+}$ subspectra, and hence valence fluctuations, are evidently absent at ~80 K.

4.2. Electrical charge transport

Bent curves of $\log\sigma$ against $1/T$, as presented in figure 4, were predicted for phonon-assisted, small-polaron hopping in disordered systems [24–26], based on different theoretical approaches. The relation that appears to describe reasonably well the curves of figure 5 in certain T ranges, originally derived by Mott [24],

$$\sigma \propto \exp[-(T_0/T)^{1/4}] \tag{1}$$

where $T_0 = c_0[\alpha^3/(k_B N(E_F))]$, $c_0 \sim 16$, $1/\alpha$ is the electron wavefunction decay constant, k_B is the Boltzmann constant, $N(E_F)$ is the density of electronic states and E_F is the Fermi energy separating occupied from non-occupied states, is valid under the conditions of electron hopping between shallow localized levels as in impurity hopping at $T \lesssim 10$ K. Later, for multiphonon-assisted, small-polaron hopping conduction between deep states in non-crystalline solids at $T < \Theta_D$ (Θ_D = Debye temperature), Emin [27] found by a non-perturbative calculation a T dependence of σ in a large T range which resembles that of equation (1); in this case it is typically $T_0 \sim 10^7$–10^{10} K. Triberis and Friedman [28] applied percolation theory to high-T multiphonon-assisted, small-polaron hopping processes in disordered systems; taking correlation effects into account they found for σ a $T^{-1/4}$ relation as in equation (1) where it is expected that $T_0 \sim 10^6$ K.

From the slopes of the curves in figure 4 we infer a rather identical value; it follows that $T_0 \sim 2 \times 10^9$ K, which is a magnitude which appears to be too high for the conditions of Mott's variable range hopping [24] and for the model of Triberis and Fiedman [28], but it is of the correct order of magnitude after Emin's model [27]. In our case, the required disorder may be provided primarily by oxygen non-stoichiometry.

An experimental $T^{-1/4}$ relation, valid up to relatively high T, has also been established for a series of compositions: amorphous Ge up to ~300 K [29], oxides $La_{2-y}Sr_yCu_{1-x}Li_xO_{4-\delta}$ up to ~300 K [30], B_4C between 10 and 300 K [31], oxygen-deficient garnets up to ~300 K [32], La_2CuO_4 up to ~300 K [33], various compositions of the spinel system $Fe_{3-x}Ti_xO_4$ up to ~430 K [10] and oxides of the system $LaNi_{1-x}Fe_xO_3$ up to ~300 K [34].

In the discussion of electrical charge transport in $Fe(Nb_{1-x}W_x)O_4$ solid solutions it has been supposed that Nb and W occur as Nb^{5+} and W^{6+} for all values of x [1]. If our samples show partly oxygen deficiency with a too high concentration of Fe^{2+}, the presence of low concentrations of Nb^{4+} and/or W^{5+} has also to be envisaged.

4.3. Thermopower Θ

If the Θ–$T^{1/2}$ relation should be applicable at low T for the results in figure 8, one can obtain further information for $T \to 0$ from the slopes of the straight lines as a function of x. A $T^{1/2}$ law has been derived for the conditions of Mott's variable range hopping $T^{-1/4}$ relation [35], but it is not clear whether, with the $T^{-1/4}$ relationship extending to much higher T, such a law follows from theory for our compositions.

In the high-T limit, for small-polaron hopping processes, when all sites have the same energy, Θ can be described by [22, 24]

$$\Theta = \frac{k_B}{|e|}\left[\ln\frac{n}{\beta(N-n)} + \alpha'\right] \tag{2}$$

where n is the concentration of hopping charge carriers, N is the concentration of available hopping sites, α' is a constant, suggested to give $<10\ \mu V\ K^{-1}$ [24] and β is the spin degeneracy factor which can take on, in general, values of 1 or 2; it is expected that $\beta = 1$ for the ferro- or ferrimagnetic state, while $\beta = 2$ is predicted for paramagnetic systems [22]. Setting $\alpha' = 0$ in a first approximation, the so-called 'Heikes' formula follows when $\beta = 1$. When electron hopping $Fe^{2+} \to Fe^{3+}$ is the decisive charge transport, it follows that $n = [Fe^{2+}]$, $N = [Fe^{2+}] + [Fe^{3+}]$, and therefore $n/(N-n) = [Fe^{2+}]/[Fe^{3+}]$. In figure 9 we present a comparison of the $[Fe^{2+}]/[Fe^{3+}]$ values inferred from low-T Mössbauer data and from high-T Θ results, using the spin degeneracy factors $\beta = 1$ or 2 for variable compositions; furthermore, theoretical values, following from the chemical formula, are given for stoichiometric samples. It should be noted that the magnetic order temperatures of the compositions under study are <80 K. For $x = 0.05$, Mössbauer results are associated with an enhanced error because of the low Fe^{2+} concentration. It has to be stressed that all Fe cations are involved in Mössbauer results while theoretically only part may be associated with conduction processes. It looks as if in figure 9 there is a rough agreement between the Mössbauer and Θ data for $x > 0.1$ when applying for Θ a value of $\beta = 2$, while for $x \lesssim 0.1$ a better agreement is given with $\beta = 1$; i.e. this interpretation means a participation of all Fe cations in charge transport. In our case, where presumably conduction occurs in chains along [001], an increasing electron correlation is to be expected for rising x that may give rise to a deviation from $\beta = 1$ or 2 in equation (2). The related issue is easily seen for compositions with x close to $x = 0.5$; in such a situation, there are only slightly more Fe^{3+} than Fe^{2+} in a chain, so thus electron hopping of the kind $Fe^{2+} \to Fe^{3+}$ can only be enabled if this process occurs simultaneously for neighbouring Fe ions because the states may be occupied (multipolaron hopping).

In this context, one should stress that according to recent literature the spin degeneracy factor β in equation (2) may take on values deviating from 2 or 1. Thus, a generalization of the 'Heikes' formula has been proposed for charge hopping effected by mixed-valence cations Me^{n+} and $Me^{(n+1)+}$ (Me = cation), based on the model of [22], with $\beta = (2S_n + 1)/(2S_{n+1} + 1)$, where S_n, S_{n+1} are cation spins [36]. For the above Fe cations, it follows, with $S(Fe^{2+}) = 2$ and $S(Fe^{3+}) = 5/2$, that $\beta = 5/6$, which is close to 1. There have been attempts to include as adequately as possible the orbital degeneracies into the calculation of the degeneracy factor β of hopping electrons for a system with mixed valencies [37].

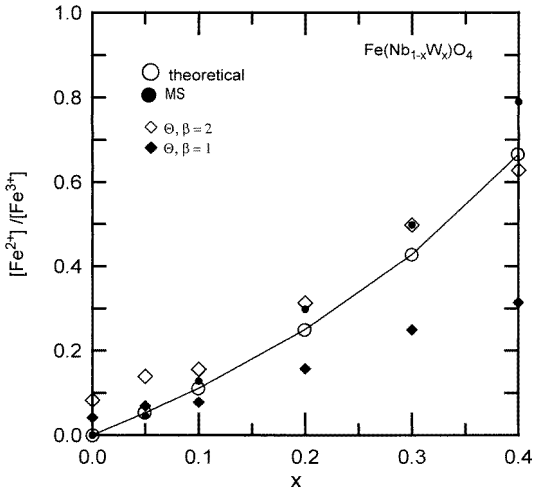

Figure 9. Concentration ratios $[Fe^{2+}]/[Fe^{3+}]$ determined from Mössbauer spectra and from thermopower Θ data (spin degeneracy factor $\beta = 1$ or 2); for comparison, theoretical values are presented for stoichiometric compositions, following from the chemical formula.

Only a qualitative picture of the energy level diagram for electron hopping has been developed thus far. For stoichiometric compositions, a low-lying full O^{2-} 2p band and empty conduction bands of Fe 4s, Nb 5s and W 6s states with intermediate d-bands are expected. From our results we infer $Fe^{2+} \rightarrow Fe^{3+}$ small-polaron hopping between deep localized states [27], far from conduction bands. In principle, a comparatively clear situation exists for compositions close to $Fe^{3+}Nb^{5+}O_4$ ($x = 0$), where theoretically a very narrow Fe^{3+} 3d and an empty Nb^{5+} 4d band may exist, which is enhanced in our polar lattice by a strong electron–lattice interaction [26]. The suggested localization of Fe^{3+} may be provided by strong disorder due to the combined action of oxygen non-stoichiometry and the effect of neighbouring Nb^{5+} and W^{6+}; at high T, a further mechanism, enhancing the localization of Fe^{3+}, is the strong electron–lattice interaction that may lead to a breakdown of the 3d band [26]. Additional Fe^{2+} in low concentrations represents impurity states acting as donors. In this conjunction an important factor can be the assumed one dimensionality of charge transport. Increasing x means an increasing concentration of Fe^{2+}, and hence of charge carriers, which gives rise to interaction effects that make the situation complex, but evidently small-polaron hopping processes occur between localized levels, as follows from experimental results.

5. Concluding remarks

The electrical DC conductivity σ, extrapolated from AC data, the thermopower Θ and ^{57}Fe Mössbauer results for polycrystalline samples $Fe^{3+}_{1-x}Fe^{2+}_{x}(Nb^{5+}_{1-x}W^{6+}_{x})O_4$, $0 \leqslant x \leqslant 0.4$, between 100 and 900 K point to a conduction mechanism that is characterized by a small-polaron hopping process $Fe^{2+} \rightarrow Fe^{3+}$, presumably along zig-zag chains of FeO_6 octahedra in the direction of the c-axis of the pseudo-rhombic lattice, which shows the following typical features.

(1) At not too low temperatures T up to ~300 K, $\log\sigma$ follows roughly a $T^{-1/4}$ relationship in analogy to Mott's variable range hopping law; this parallels the behaviour

$\Theta \propto T^{1/2}$ that is expected for this kind of hopping. The $T^{-1/4}$ behaviour of σ up to ~300 K is valid after Emin [27] for multiphonon-assisted electron hopping processes between deep states in disordered lattices that may be brought about in our case predominantly by oxygen non-stoichiometry.

(2) Above ~300 K, no values of σ for the crystal could be gained from polycrystalline samples. In this T range, Θ for all compositions is T-independent and from equation (2) the concentration ratio of Fe^{2+}/Fe^{3+} could be determined for those Fe taking part in charge transport; this ratio is roughly compatible with that determined from ^{57}Fe Mössbauer data, which encompasses all Fe cations. This result means that practically all Fe are involved in electron hopping $Fe^{2+} \rightarrow Fe^{3+}$. For larger x, and hence Fe^{2+} concentrations, electron correlation effects are probable.

In order to elucidate the suggested one-dimensional conduction in more detail, measurements on single crystals are in progress.

Acknowledgments

The author is grateful to Dr J Schneider, Institut für Kristallographie und Mineralogie der Universität München, for help regarding the x-ray Rietveld refinement technique. The author is indebted to Professor E Umlauf, Tieftemperatur-Institut der Bayer. Akademie der Wissenschaften, for a critical review of the manuscript. Thanks are due to the Deutsche Forschungsgemeinschaft for financial support.

References

[1] Noda Y, Shimada M, Koizumi M and Kanamaru F 1979 *J. Solid State Chem.* **28** 379
[2] Yamada T 1973 *J. Phys. Soc. Japan* **3** 130
[3] Ramdani R, Gleitzer C, Gavoille G, Cheetham A K and Goodenough J B 1985 *J. Solid State Chem.* **60** 269
[4] Reddy P Y and Rao T S 1985 *Phys. Status Solidi* a **92** 303
[5] Whall T, Salerno N, Proykova Y, Mirza K A and Mazen S 1986 *Phil. Mag.* B **53** L107
[6] Ahmet M A, El-Nimr M K, Tawfik A and El-Hasab A M 1991 *Phys. Status Solidi* a **123** 501
[7] Kozlowski A, Rasmussen R J, Sabol J E, Metcalf P and Honig J M 1993 *Phys. Rev.* B **48** 2057
[8] Carter D C and Mason T O 1988 *J. Am. Ceram. Soc.* **71** 213
[9] Gillot B and Nohair M 1995 *Phys. Status Solidi* **148** 239
[10] Brabers V A M 1995 *Physica* B **205** 143
[11] Grandjean F and Gerard A 1982 *Valence Instabilities* ed P Wachter and H Boppard (Amsterdam: North-Holland) p 587
[12] Garg K B, Chauhan H S, Chandra U, Jerath K S and Grandjean F 1987 *Solid State Commun.* **62** 575
[13] Ülkü D 1967 *Z. Kristallogr.* **124** 192
[14] Cid-Dresdner H and Escobar C 1968 *Z. Kristallogr.* **127** 61
[15] Schmidbauer E and Schneider J 1997 *J. Solid State Chem.* **134** 253
[16] Lotgering F K and Van Diepen A M 1977 *J. Phys. Chem. Solids* **38** 565
[17] Eibschütz M, Ganiel U and Shtrikman S 1967 *Phys. Rev.* **156** 259
[18] Macdonald J R 1987 *Impedance Spectroscopy* (New York: Wiley)
[19] Moore J P and Graves R S 1973 *J. Appl. Phys.* **44** 1174
[20] Gold A V, MacDonald D K C, Pearson W B and Templeton I M 1960 *Phil. Mag.* **5** 765
[21] Schmidbauer E, Schanz U and Yu F J 1991 *J. Phys.: Condens. Matter* **3** 5341
[22] Chaikin P M and Beni G 1979 *Phys. Rev.* B **13** 647
[23] Mott N F and Davis D A 1971 *Electronic Processes in Non-Crystalline Materials* (Oxford: Clarendon)
[24] Austin I G and Mott N F 1969 *Adv. Phys.* **18** 41
[25] Mott N F 1969 *Phil. Mag.* **19** 835
[26] Schnakenberg J 1968 *Phys. Status Solidi* **28** 6232
[27] Emin D 1974 *Phys. Rev. Lett.* **32** 303
[28] Triberis G P and Friedman L R 1985 *J. Phys. C: Solid State Phys.* **18** 2281

[29] Pollak M, Knotek M L, Kurtzman H and Glick H 1973 *Phys. Rev. Lett.* **30** 856
[30] Kastner M A *et al* 1988 *Phys. Rev.* B **37** 111
[31] Zuppiroli L and Forro L 1989 *Phys. Lett.* **141** 181
[32] Barbara B, Bechevet B, Sampaio L C and Armand M F 1992 *J. Magn. Magn. Mater.* **116** 61
[33] Lunkenheimer P, Resch M, Loidl A and Hidaka Y 1992 *Phys. Rev. Lett.* **69** 498
[34] Chainani A, Sarma D D, Das I and Sampathkumaran E V 1996 *J. Phys.: Condens. Matter* **8** L631
[35] Zvyagin I P 1978 *Sov. Phys.–Semicond.* **12** 606
[36] Doumerc J-P 1994 *J. Solid State Chem.* **110** 419
[37] Marsh D B and Parris P E 1996 *Phys. Rev.* B **54** 7720